Simulation and Experimental Evaluation of the Contribution of Biarticular Gastrocnemius Structure to Joint Synchronization in Human-Inspired Three-Segmented Elastic Legs

Dorian Scholz[†], Christophe Maufroy[⋆], Stefan Kurowski[†], Katayon Radkhah[†], Oskar von Stryk[†], André Seyfarth[⋆]

[†] Fachgebiet Simulation, Systemoptimierung und Robotik
Technische Universität Darmstadt, Department of Computer Science
Hochschulstr. 10, D-64289 Darmstadt, Germany
{scholz, kurowski, radkhah, stryk}@sim.tu-darmstadt.de,
WWW home page: http://www.sim.tu-darmstadt.de

[⋆] Lauflabor Locomotion Laboratory
Technische Universität Darmstadt, Institut für Sportwissenschaft
Magdalenenstr. 27, D-64289 Darmstadt, Germany
{cmaufroy, seyfarth}@sport.tu-darmstadt.de,
WWW home page: http://www.lauflabor.de

Abstract. The humanoid robot BioBiped2 is powered by series elastic actuators (SEA) at the leg joints. As motivated by the human muscle architecture comprising monoarticular and biarticular muscles, the SEA at joint level are supported by elastic elements spanning two joints. In this study we demonstrate in simulation and in robot experiments, to what extend synchronous joint operation can be enhanced by introducing elastic biarticular structures in the leg, reducing the risk of over-extending individual joints.

1 Introduction

During bouncing gaits such as hopping and fore-foot running, the three-segmented human leg is loaded and unloaded during contact time while pivoting around the ball of the foot [1]. This observation contrasts with the current state-of-the-art running biped robots, which either run with their feet flat on the ground (such as ASIMO [2]) or have no foot at all and are equipped with pogo-stick [3] or two-segmented [4] legs. While this latter strategy is reasonable for running, it may be problematic for other gaits, such as walking and standing, where the role of the ankle-foot complex becomes important for posture control and energy injection (during the late stance push-off). This explains why many walking robots (such as [2][5]) have feet. Hence, the previous argument suggests that humanoid robots aiming at multimodal locomotion should be equipped with three-segmented legs. A better understanding of the dynamic operation of this type of leg structure,

especially during bouncing gaits, would help in exploiting the benefits of this leg design.

In addition to segmentation, compliance is another key aspect of human leg operation. Elastic leg operation is widely observed in human locomotion [6] and biomechanical models suggest that this property may provide the mechanical basis of hopping, running and walking [7][8][9]. The elasticity of the leg as a whole is supported by elastic operation at the level of the individual joints, primarily ankle and knee [1][6]. These observations have fuelled the development of compliant actuators, including the series elastic actuators [10], and the progressive shift of compliance from the leg level (as in Raibert's hoppers [3]) to the joint level (as in M2V2 [11] or BioBiped1 [12]) in legged robots. However, the implementation of compliance at the joint level comes with the challenge of maintaining the leg's configurational stability. Using stability analysis in the static case, Seyfarth et al. [13] pointed out the risk of bifurcations from usual zigzag leg configuration to bow leg configuration, in which either the knee or ankle joints is overextended.

In the dynamic case, similar concerns related to the over-extension of one of the joints exist during the loading and unloading phases of the three-segmented leg in bouncing gaits. This risk could be mitigated by finding the properties of the elastic structures acting at the knee and ankle that can guarantee robust synchronous operation of these joints such as observed in human hopping [14]. This is precisely the goal of this paper. In addition to monoarticular structures, a biarticular elastic structure, mimicking the human gastrocnemius muscle, is considered. Our hypothesis, motivated by the known role of biarticular muscles in inter-joint coordination in humans [15][16], is that the use of biarticular structures like the gastrocnemius can increase the robustness of the behavior with respect to initial leg configurations and the spring stiffness ratio of the monoarticular structures. This is particularly important when it comes to real world application of the robot, where precise adjustments of these quantities are difficult to achieve, due to sensor and modeling inaccuracies as well as environmental factors, such as not perfectly flat ground, leading to variable foothold position.

2 Simulation and experimental setup

2.1 Experimental framework

In this paper, passive rebound experiments were used as a simplified experimental framework to investigate the influence of the passive elastic structures in the segmented leg during hopping. The robot was dropped from a given height, landed with its foot tips vertically aligned with the hip joint and the subsequent rebound, resulting only from the action of the passive elastic leg structures, was observed. These experiments were performed on the BioBiped2 robot (see Fig. 1c) and in simulation using an approximate model of robot. The BioBiped2 is a revised version of BioBiped1 described in [12], which was improved compared to its predecessor in many electronic and mechanical design details. For
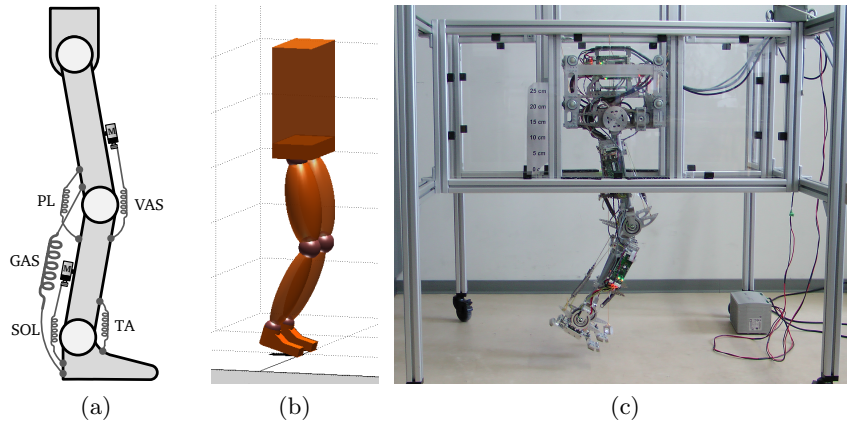
Fig. 1: (a) Elastic structures used during the passive rebound experiment (b) Snapshot of the BioBiped simulation model (c) BioBiped2 in the experimental setup for the robot experiments

the experiments presented here, the main improvement is the usage of ball bearings in the joints, drastically reducing the friction and allowing for an easier investigation of the elastic mechanism.

For simplicity, the trunk motion of the robot was constrained to vertical motions and only elastic structures at the knee and ankle joint were considered (see Fig. 1a). At knee and ankle joints, the motor positions of the series elastic actuators, playing the role of the extensor muscles (VAS and SOL), were set to balance the joint torques generated by the passive flexor structures (PL and TA) in the initial leg configuration. Their position was subsequently held constant so that the generated torques at the knee and ankle were only the result of the passive elastic structures. To gain insight in the effect of the gastrocnemius structure (GAS), every experiment was performed twice: with and without a simplified GAS, implemented as a linear spring (see Table 1) connecting heel and thigh. It was mounted to be at its rest length in the initial leg configuration at touch-down.

The model of the robot, implemented and simulated using the framework presented in [17], is represented in Fig. 1b. The simulation model parameters are summarized in the Appendix, in Table 2. For simplicity, we consider that the joints are frictionless and that no energy dissipation occurs in the elastic structures.

The setup for the robot experiments is depicted in Fig. 1c. The constraint on the trunk motion is achieved using a frame that prevents all but the vertical motion, while rollers attached to the robot insure low friction along that direction.

2.2 Joint synchronization index
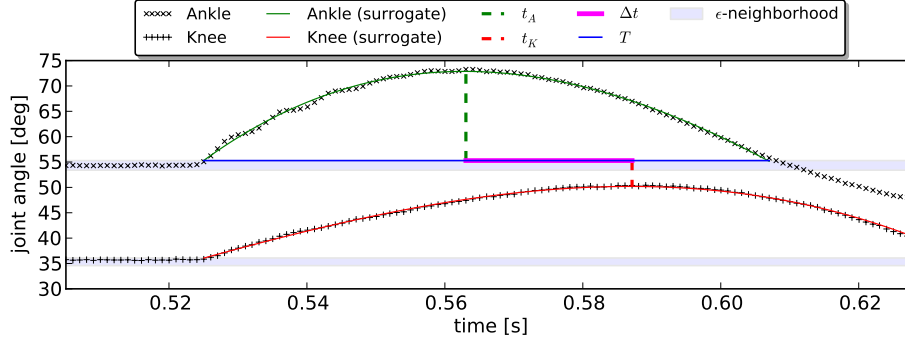
Fig. 2: Visualization of the joint trajectories during one of the robot experiments. Besides the actual measurement data, the graph shows the surrogate functions, the total time T between leaving the ϵ-neighborhood and reentering it and the time difference Δt between the trajectories' maxima (t_A, t_K).

The synchronization of the knee and ankle movements was quantified using the phase difference $\Delta\phi$ between the flexion-extension motions of these two joints, as given by the following equation:

$$\Delta\phi = |\frac{t_K - t_A}{T}| = |\frac{\Delta t}{T}|$$

where t_K and t_A are respectively the instants when the knee and the ankle are maximally flexed during contact, while T is the time, measured from landing, until either joint angle reaches its original landing value (see Fig. 2). For the estimation of t_K and t_A in the robot experiments, the data around the maximal flexion peak was approximated by a surrogate function (6th order, generated by regression using 40 data points) to reduce the influence of measurement noise. The measurement data together with the surrogate function for an example trajectory are displayed in Fig. 2. To enhance the robustness of phase-length detection, an ϵ-neighborhood was introduced around the value of the landing angle and T was defined for all experiments as the time from leaving this ϵ-neighborhood until the first trajectory reenters it. The value of ϵ was set to 5% of the difference between the landing angle and maximum flexion angle.

2.3 Parameter space

The influence of the following two parameters on knee and ankle joint synchronization was investigated:

– the spring stiffness ratio $R = k_{\mathrm{SOL}}/k_{\mathrm{VAS}}$

– the joint angle difference at landing $\Delta\theta = \theta_{K,0} - \theta_{A,0}$

where k stands for the linear stiffness of the elastic structures and the indices K and A refer to the knee and ankle joints, respectively.

The other parameters were kept constant during all experiments. Although the initial leg configuration was variable and dependent on $\Delta\theta$, the joint angles were chosen to maintain the total initial leg length L_0 (distance from hip joint to foot tip) at a constant fraction of the maximum leg length L_{max} (sum of all leg segment lengths). The value of the initial leg length L_0 was set to the average value found in humans at preferred hopping frequency as described in [18]. Similarly, k_{SOL} was set constant, while k_{SOL} was computed based on the spring stiffness ratio R. The value of k_{VAS} was chosen to results in similar maximal leg compression as during human hopping (i.e. about 10% of L_{max}).

The values of the constant parameters are given in the upper part of Table 1. The lower part of Table 1 shows the values of the stiffness ratio R and the angle difference $\Delta\theta$ used in the robot experiments. Every combination of these configurations was tested on the robot with and without the gastrocnemius structure GAS. In simulation, many more configuration within the same parameter range were tested to produce more fine grained results.

Constant parameters							
L_{max}	[m]	0.727	k_{VAS}	[N/mm]	15.5	$F_{0_{\mathrm{VAS}}}$	[N]	36.8
L_0	[m]	0.94 L_{max}	k_{GAS}	[N/mm]	7.9	$F_{0_{\mathrm{GAS}}}$	[N]	27.6
			$k_{\mathrm{PL/TA}}$	[N/mm]	4.1	$F_{0_{\mathrm{PL/TA}}}$	[N]	13.8

Stiffness ratio R in robot experiments						
Experiment		A	B	C	D	E
R	[-]	0.265	0.432	0.510	0.839	1.155
k_{SOL}	[N/mm]	4.1	6.7	7.9	13.0	17.9
$F_{0_{\mathrm{SOL}}}$	[N]	13.8	22.6	27.6	27.6	58.9

Angle difference $\Delta\theta$ in robot experiments						
Experiment		1	2	3	4	5
$\Delta\theta$	[deg]	-7	-0.5	6.6	14.8	24.7
knee $\theta_{K,0}$	[deg]	138	139.5	141.6	144.8	149.7
ankle $\theta_{A,0}$	[deg]	145	140	135	130	125

Table 1: Constant and variable parameters used during the experiments: leg lengths L_{max} and L_0, spring stiffnesses k and pretensions F_0, spring stiffness ratios R and joint angles θ.

3 Results and discussion

In this study the effect of GAS on synchronous joint operation in a three-segmented leg is studied in simulation and compared to robot experiments with BioBiped2.

The phase difference $\Delta\phi$, represented in Fig. 3 as a function of the stiffness ratio R and the initial leg configuration, is characterized by the angle difference at landing $\Delta\theta$. The results are shown without and with the GAS structure attached for simulation (Fig. 3a and 3b) and robot experiments (Fig. 3c and 3d).

The simulation results show that, even without the GAS structure, synchronous operation of the knee and ankle joints is possible in most of the range considered for the angle difference $\Delta\theta$. However, this requires a fine adjustment of the stiffness ratio R to fall in the thin white region of Fig. 3a. This is particularly true for small values of $\Delta\theta$ (i.e. the landing configuration with congruent knee and ankle angles) where the sensitivity with respect to R appear to be the largest. On the other hand, the synchronous operation becomes less sensitive to variation of R as the angle difference $\Delta\theta$ increases. This situation corresponds to a landing configuration with extended knee and flexed ankle, which is favored by humans [18].

Adding the GAS structure has a considerable influence on the results (Fig. 3b). The parameter region where synchronous joint operation occurs with $\Delta\phi < 0.05$ is considerably enlarged. Hence, the sensitivity of the behavior with respect to the stiffness ratio R is greatly reduced, especially for large angle differences $\Delta\theta$. This allows the system to potentially operate with various overall leg stiffness, by varying the stiffness ratio R, while preserving the joint synchronization. In addition, the risk of heel strike leading to energy dissipation due to the impact with the ground is reduced (see magenta area in Fig. 3).

Some of the tendencies observed in simulations are found in the results of the robot experiments. Generally, synchronous operation is improved when the angle differences $\Delta\theta$ is positive. Additionally, good joint synchronization is possible (with phase differences $\Delta\phi < 0.10$), even without GAS structure (see Fig. 3c), but the synchronization is notably improved by the addition of the GAS structure. It also reduces the risk of heel strike.

Besides these common tendencies, the results for the robot experiments present specific features worth to discuss. First, the region of parameters resulting in low phase differences ($\Delta\phi < 0.20$) without the GAS structure is much more extended than in the simulations. As a result, the effect of the addition of GAS is not as pronounced as for the simulation results.

Another discrepancy between the robot experiments and the simulations is the spring model. In simulation a linear extension springs without pretension in used. In reality, the extension springs are not perfectly linear and have a significant pretension (see values for F_0 in Table 1). Hence, the apparent stiffness of the spring is altered and the ratio computed using the nominal spring stiffnesses may not reflect this change. This could potentially explain why low phase differences are observed in the robot experiments for much lower values of R than in the simulations.
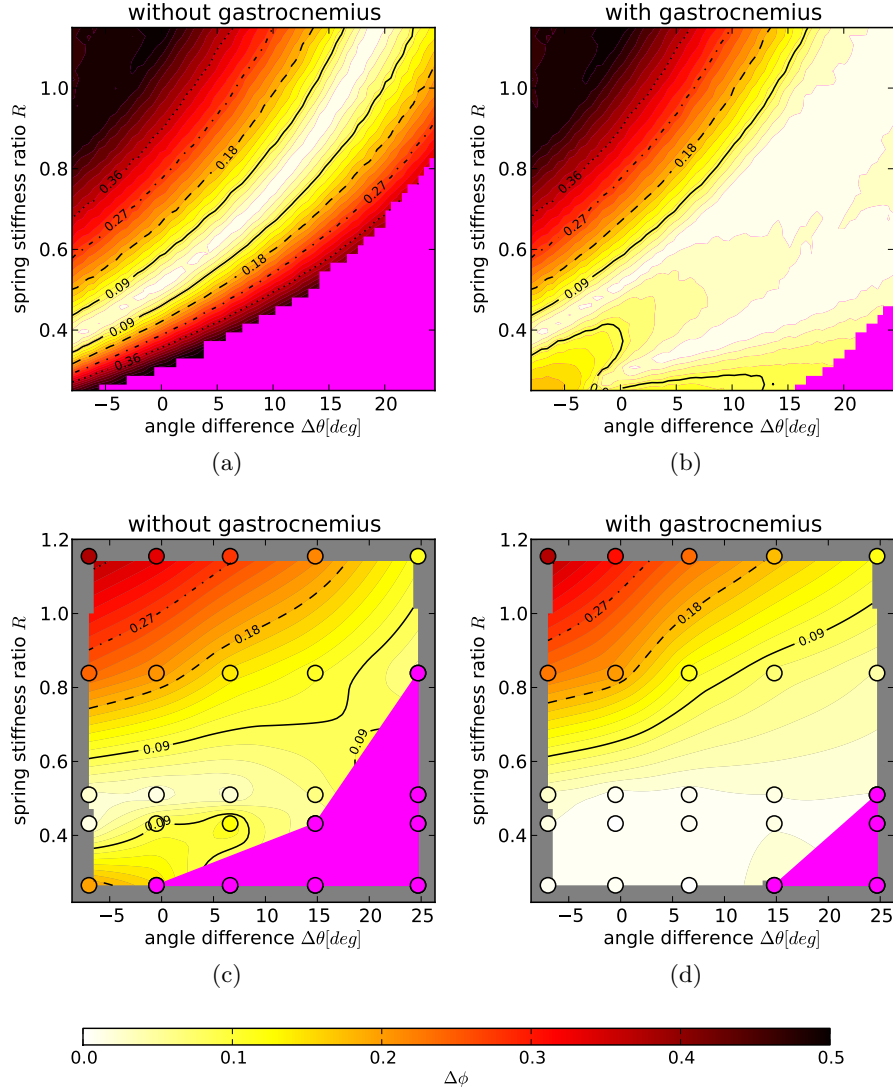
Fig. 3: Phase differences of knee and ankle joints in the simulation (3a, 3b) and in the robot experiments (3c, 3d) each without and with GAS. The trials where heel contact occurred during the stance phase are located in the lower right corner in both simulation and experiments and are marked in magenta. The configurations used for the 25 robot experiments (black circles) are shown in Table 1 and the angles' definitions in Fig. 4 (Appendix). As these configurations are not equidistant in the graph the $\Delta\phi$ values in-between the experiments have been linearly interpolated for easier comparison with the simulation results.

4 Conclusions and future work

The results in Fig. 3 show that it is possible to achieve synchronized joint movements without gastrocnemius. But the corresponding parameter region is quite limited, in the simulation (Fig. 3a) as well as on the real robot (Fig. 3c). The in-phase operation of knee and ankle joints can be supported by an elastic biarticular structure (GAS) mimicking the function of the human gastrocnemius muscle. This was demonstrated in simulation and for the BioBiped2 robot as can be seen in Fig. 3b and Fig. 3d. More specifically the phase difference was reduced for every leg configuration tested on the robot, thus making it possible to get synchronized joint movements even without perfect touchdown conditions. Interestingly, the range of in-phase joint operation was even larger in the robot than predicted by the simulation model. This indicates, that other effects (e.g. joint damping) may further facilitate synchronous joint function. When looking at robots in real world scenarios variations in leg configurations are inevitable. The additional robustness gained through the biarticular structure against changes in leg configuration could help in solving the challenges of bipedal walking on rough terrain and unstructured environment.

Furthermore this additional robustness opens the possibility to reduce the effort in terms of sensory feedback and energy input on joint level while still achieving equally good overall leg performance. Another way of looking at this is the shift of parts of the control to the distribution of elastic structures and actuators in the segmented body.

In future work, the influence of the springs pretension on the results could be investigated by using overextended springs. Additionally, the evaluation, focused so far to the knee and ankle joints, will be extended to the hip joints. For that purpose, the constraints on the trunk will be relaxed and the elastic structures spanning this joint will be added. Yet another avenue of research will be to investigate how the benefits of the biarticular structures shown here in the passive case translate to an actively controlled motion. One interesting aspect would be the possibility to reduce the control effort and the energy consumption necessary for synchronous joint operation, i.e. in continuous hopping.

References

1. M. Guenther and R. Blickhan. Joint stiffness of the ankle and the knee in running. *J Biomech*, 35:1459–1474, 2002.
2. Asimo webpage: http://world.honda.com/asimo/.
3. M.H. Raibert. *Legged Robots that Balance.* MIT Press, Cambridge MA, 1986.

4. J.W. Hurst. *The Role and Implementation of Compliance in Legged Locomotion.* PhD thesis, The Robotics Institute, Carnegie Mellon University, Pittsburgh PA, 2008.
5. Petman webpage: http://www.bostondynamics.com/robot_petman.html.
6. S.W. Lipfert. *Kinematic and Dynamic Similarities between Walking and Running.* Verlag Dr. Kovac, Hamburg, 2010.
7. R. Blickhan. The spring-mass model for running and hopping. *Journal of Biomechanics*, 22:1217–1227, 1989.
8. A. Seyfarth, H. Geyer, M. Guenther, and R. Blickhan. A movement criterion for running. *J Biomech.*
9. H. Geyer, A. Seyfarth, and R. Blickhan. Compliant leg behaviour explains basic dynamics of walking and running. *Proc. Royal Society B: Biological Sciences*, 273:2861–2867, 2006.
10. G. A. Pratt and M. M. Williamson. Series elastic actuators. In *Proc. IEEE International Workshop on Intelligent Robots and Systems*, pages 399–406, 1995.
11. J. Pratt and B. Krupp. Design of a bipedal walking robot. In *Proceedings of the 2008 SPIE*, volume 6962.
12. K. Radkhah, C. Maufroy, M. Maus, D. Scholz, A. Seyfarth, and O. von Stryk. Concept and design of the biobiped1 robot for human-like walking and running. *International Journal of Humanoid Robotics*, 8(3):439–458, 2011.
13. A. Seyfarth, M. Guenther R., and Blickhan. Stable operation of an elastic three-segmented leg. *Biol. Cybern.*, 84:365–382, 2001.
14. S. Rapoport, J. Mizrahi, E. Kimmel, O. Verbitsky, and E. Isakov. Constant and variable stiffness and damping of the leg joints in human hopping. *J Biomech Eng*, 125(4):507–514, 2003.
15. F.E. Zajac. Muscle coordination of movement: a perspective. *J Biomech*, 26:109–124, 1993.
16. G.J. van Ingen Schenau, C.A. Pratt, and J.M. Macpherson. Differential use and control of mono- and biarticular muscles. *Human Movement Science*, 13(3-4):495–517, 1994.
17. T. Lens, K. Radkhah, and O. von Stryk. Realistic contact forces for manipulators and legged robots with high joint elasticity. In *Proc. 15th International Conference on Advanced Robotics (ICAR)*, pages 34–41, 2011.
18. C.T. Farley and D.C. Morgenroth. Leg stiffness primarily depends on ankle stiffness during human hopping. *J Biomech*, 32:267–273, 1999.

5 Appendix
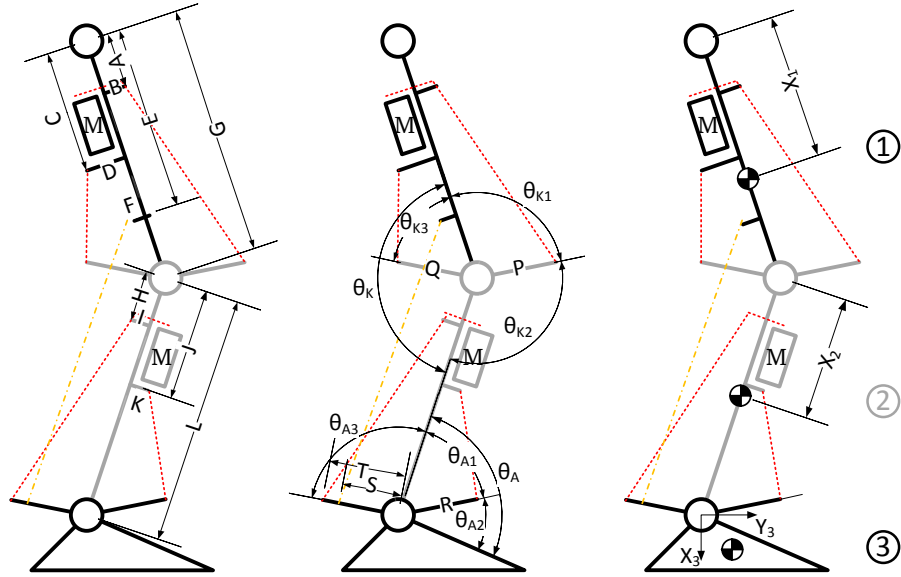
Fig. 4: Dimensions of the BioBiped2 leg. Corresponding values are listed in Table 2.

Measurement	Value	Unit	Measurement	Value	Unit
A	0.080	[m]	K	0.058	[m]
B	0.018	[m]	L	0.330	[m]
C	0.226	[m]	P	0.068	[m]
D	0.070	[m]	Q	0.038	[m]
E	0.226	[m]	R	0.023	[m]
F	0.070	[m]	S	0.053	[m]
G	0.330	[m]	T	0.061	[m]
H	0.076	[m]	θ_{K2}	155	[deg]
I	0.022	[m]	$\theta_{A1} + \theta_{A2} + \theta_{A3}$	213	[deg]
J	0.210	[m]			

Table 2: Values of the dimensions represented in Fig. 4. These values are also used in the simulation model.